Aerodynamics of a Letterbox Trailing Edge: Effects of Blowing Rate, Reynolds Number, and External Turbulence on Aerodynamic Losses and Pressure Distribution

N. J. Fiala
EERC,
University of North Dakota,
Grand Forks, ND 58202

J. D. Johnson
United States Air Force,
518 Combat Sustainment Squadron,
Hill AFB, UT 84056

F. E. Ames
Department of Mechanical Engineering,
University of North Dakota,
Grand Forks, ND 58202

A letterbox trailing edge configuration is formed by adding flow partitions to a gill slot or pressure side cutback. Letterbox partitions are a common trailing edge configuration for vanes and blades, and the aerodynamics of these configurations are consequently of interest. Exit surveys detailing total pressure loss, turning angle, and secondary velocities have been acquired for a vane with letterbox partitions in a large-scale low speed cascade facility. These measurements are compared with exit surveys of both the base (solid) and gill slot vane configurations. Exit surveys have been taken over a four to one range in chord Reynolds numbers (500,000, 1,000,000, and 2,000,000) based on exit conditions and for low (0.7%), grid (8.5%), and aerocombustor (13.5%) turbulence conditions with varying blowing rate (50%, 100%, 150%, and 200% design flow). Exit loss, angle, and secondary velocity measurements were acquired in the facility using a five-hole cone probe at a measuring station representing an axial chord spacing of 0.25 from the vane trailing edge plane. Differences between losses with the base vane, gill slot vane, and letterbox vane for a given turbulence condition and Reynolds number are compared providing evidence of coolant ejection losses, and losses due to the separation off the exit slot lip and partitions. Additionally, differences in the level of losses, distribution of losses, and secondary flow vectors are presented for the different turbulence conditions at the different Reynolds numbers. The letterbox configuration has been found to have slightly reduced losses at a given flow rate compared with the gill slot. However, the letterbox requires an increased pressure drop for the same ejection flow. The present paper together with a related paper (2008, "Letterbox Trailing Edge Heat Transfer—Effects of Blowing Rate, Reynolds Number, and External Turbulence on Heat Transfer and Film Cooling Effectiveness," ASME, Paper No. GT2008-50474), which documents letterbox heat transfer, is intended to provide designers with aerodynamic loss and heat transfer information needed for design evaluation and comparison with competing trailing edge designs. [DOI: 10.1115/1.3195035]

1 Introduction

Trailing edge cooling designs typically balance tradeoffs between aerodynamic efficiency and heat transfer effectiveness. The present paper investigates aerodynamic losses for a letterbox vane configuration over a range of exit chord Reynolds numbers (500,000, 1,000,000 and 2,000,000), inlet turbulence levels (0.7%, 8.5%, and 13.5%), and trailing edge discharge flow rates (50%, 100%, 150%, and 200% of design). In a related paper [1] heat transfer and adiabatic effectiveness levels are examined for the partitions and inner suction surface downstream from the trailing edge discharge slot. This research builds on earlier work documenting gill slot vane and base vane aerodynamics. The comprehensive aerodynamic loss and heat transfer measurements for the present letterbox vane and previous gill slot vane are expected to provide a basis to assess heat transfer and aerodynamic performance of these designs.

Contributed by the International Gas Turbine Institute of ASME for publication in the JOURNAL OF TURBOMACHINERY. Manuscript received May 25, 2009; final manuscript received May 26, 2009; published online May 4, 2010. Review conducted by David Wisler. Paper presented at the ASME Turbo Expo 2008: Land, Sea and Air (GT2008), Berlin, Germany, June 9–13, 2008.

The present exit survey measurements were acquired using a conventional five-hole cone probe, which was traversed at a position about one-quarter axial chord downstream of the vane trailing edge plane. Measurements were taken over the full range of Reynolds numbers, turbulence conditions, and a more limited range of coolant discharge flow rates. Total pressure loss and secondary velocities have been documented in well resolved contour and vector plots. Total pressure loss coefficients and turning angle have been mass averaged across the passage and presented in terms of spanwise distributions. Passage averaged total pressure loss and turning angle have been tabulated for all conditions surveyed.

2 Background

Denton [2] suggested that historically loss in turbines has been broken down into "profile loss," "endwall loss," and "leakage loss" but suggested that these loss mechanisms are seldom independent. He further stated that mixing losses are not confined to boundary layers. Glassman [3] indicated that the chief source of profile losses on vanes and blades is boundary layer growth and separation from the trailing edge. He suggested that trailing edge losses correlate closely with trailing edge thickness and shape.

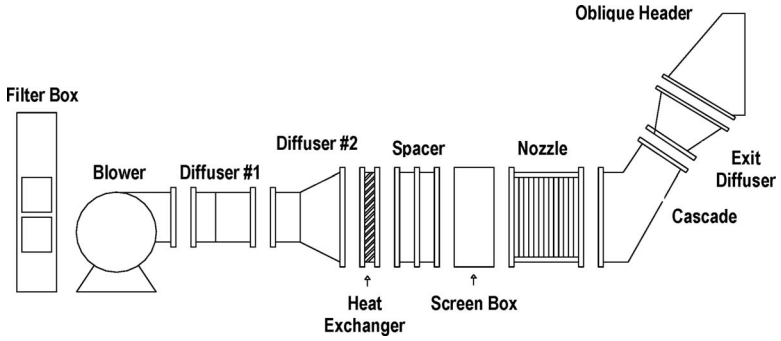

Fig. 1 Schematic of large-scale incompressible flow vane cascade wind tunnel

Gregory-Smith and Cleak [4] studied the influence of grid turbulence on losses in a turbine cascade. While they found about a 7% increase in the midspan loss coefficient with the grid turbulence, they also found about a 12% decrease in the endwall loss coefficient. Slightly over half of this reduction could be attributed to the thinner inlet boundary layer of the grid turbulence condition. However, even accounting for inlet boundary layer loss they noted a reduction in the endwall loss with the grid turbulence. Ames and Plesniak [5] studied the influence of simulated aerocombustor turbulence on two-dimensional exit losses in a turbine vane cascade and measured a total pressure loss or "background loss" between wakes. Turbulence measurements performed by Ames [6] noted that from the inlet to the exit of the cascade, turbulent kinetic energy and dissipation remained approximately constant. Assuming production was equal to dissipation, then about 1/3 of these background losses could be attributed to turbulent mixing outside boundary layers and wakes. This suggests that the other 2/3 of this background loss is due to redistribution of wake and endwall losses by turbulent mixing.

Denton [2] indicated that endwall loss is the most difficult loss component to understand and to predict. A substantial proportion of total passage losses is due to the loss generated from the endwall flow. Loss mechanisms include endwall boundary layer growth, boundary layer separation and the generation, growth, and mixing of endwall vortices. Sieverding [7] provided a well referenced review of secondary flows in turbine passages. In his review he presented the secondary flow models of both Klein [8] and Langston et al. [9]. The model of Langston et al. included suction and pressure side legs of the horseshoe vortex system generated at the leading edge of the vane as well as the passage vortex. Sieverding [7] suggested that the suction side corner vortex originates from the interaction of the passage vortex with the suction surface. Marchal and Sieverding [10] found an increasing growth of endwall losses downstream from the region of maximum velocity. However, vortex systems have often been reported with much more complexity than the basic components suggested above. For example, Praisner and Smith [11] presented a horseshoe vortex system including horseshoe, secondary, tertiary, and corner vortices.

Recent work has been undertaken to reduce the aerodynamic and heat transfer impact of secondary flows on endwalls. Burd and Simon [12] used endwall contouring to reduce the impact of secondary flows. Zess and Thole [13] investigated the use of leading edge fillets with a similar effect. Ingram et al. [14] controlled the cross-passage pressure gradient with endwall profiling and was able to reduce endwall losses by 24%.

Kapteijn et al. [15] investigated the transonic performance of a cutback and covered trailing edge with injection. They found higher turning and higher losses with the pressure side cutback than the covered trailing edge. Osnaghi et al. [16] investigated aerodynamic losses due to a combination of trailing edge discharge, suction and pressure surface film cooling, and showerhead film cooling. The trailing edge, which discharged through rectangular holes, comprised 38% of the flow at design and generated about 50% of the total loss increase above the base vane. The design flow thermodynamic loss was about 50% above the solid vane. Pappu and Schobeiri [17] defined an energy based loss coefficient and tested two turbine blade designs with trailing edge injection finding loss that was minimized when the coolant discharge to exit plane velocity ratio was 1. Deckers and Denton [18] tested a flat plate model airfoil with trailing edge injection. They found that a modest amount of injection reduced the kinetic energy loss coefficient and that the optimum coolant total to base pressure ratio increased with increasing exit plane Mach number. Uzol and Camci [19] investigated total pressure losses for a blade with trailing edge coolant discharge and coolant discharge through a pressure side cutback. They found increasing losses with increasing flow rates up to 3% of mainstream flow but found that losses decreased at 5% mainstream flow for both geometries. They found that the pressure side cutback had lower losses than the blade with a full trailing edge. Telisinghe et al. [20] investigated kinetic energy losses for a plate with a conventional trailing edge and a cutback, which was formed in the envelope of the conventional trailing edge. Generally, they found a similar zero blowing loss coefficient for the cutback and the trailing edge discharge. However, at increasing blowing ratios they found that the cutback had a greater loss than the data plate. Brundage et al. [21] investigated trailing edge aerodynamic losses for trailing edge discharge in a trailing edge cooling model. They found that the base pressure drag was minimized at 2.1% blowing.

In a related study, Ames et al. [22] investigated the influence of turbulence condition and Reynolds number on the present base vane aerodynamics. They found increasing total passage loss with increasing turbulence level and decreasing Reynolds number. Ames et al. [23] also investigated the influence of blowing rate, Reynolds number, and external turbulence on aerodynamic losses for the present vane profile configured with a gill slot trailing edge. In the present paper, results for the letterbox vane are compared with measurements for the gill slot and base vane.

3 Experimental Approach

The present study investigated letterbox vane exit total pressure losses and secondary flows as a basis to compare the aerodynamic efficiency of competing trailing designs. Letterbox vane aerodynamic losses were acquired over a range of exit chord Reynolds numbers, turbulence conditions, and coolant flow rates using a large-scale low speed wind tunnel with a large-scale cascade test section.

3.1 Wind Tunnel. The large-scale low speed wind tunnel is shown schematically in Fig. 1. The wind tunnel is driven by a large blower, which can generate a volumetric flow rate of 6.6 m^3/s with a 5000 Pa pressure rise. The blower entrains air through a large filter box into the blower inlet and discharges

Table 1 Characteristics of inlet turbulence for low, grid, and aerocombustor conditions

	Reynolds	Tu	U (m/s)	Lx (cm)	Lu (cm)	ε (m^2/s^3)
Low turbulence (LT)	500,000	0.0069	4.96	8.12	127.0	0.00005
	1,000,000	0.0076	10.43	5.02	154.5	0.00035
	2,000,000	0.0060	18.71	3.58	15.5	0.0144
Aeroderivative combustor (AC)	500,000	0.1313	5.24	3.68	7.24	6.67
	1,000,000	0.1402	9.32	3.52	6.36	51.5
	2,000,000	0.1339	18.39	3.58	7.35	302.0
Grid (Grid)	500,000	0.0821	4.77	2.00	3.27	2.70
	1,000,000	0.0861	10.19	2.04	3.35	29.8
	2,000,000	0.0884	19.27	2.35	3.53	206.8

through a two-stage multivane diffuser. The diffuser directs the air through a water cooled heat exchanger, which keeps the tunnel air temperature constant. The air is then directed through a rectangular spacer into a flow conditioning section consisting of four fine mesh nylon screens, which reduce any lateral velocity variations. The screen box directs the air into a 3.6– 1 area ratio nozzle, which further enhances the inlet uniformity of the flow. The nozzle in turn directs air into the large-scale cascade test section. A two-axis traversing system equipped with a five-hole cone probe is connected with the outlet of the cascade test section. The traversing system exhausts into a multivane exit diffuser used to recover pressure and extend the Reynolds number range of the wind tunnel. The flow is then directed into an oblique header used to direct the air away from the ceiling.

3.2 Turbulence Conditions. Three turbulence conditions were generated for this present study and included a low turbulence condition (LT), a grid generated turbulence condition (GR), and an aerocombustor turbulence condition (AC). The low turbulence condition was generated by the combination of screen box and nozzle shown schematically in Fig. 1 and generates a nominal turbulence level of 0.7%. The characteristics of the turbulence generated by the low, grid, and aerocombustor turbulence configurations are presented in Table 1. These measurements were taken using access ports placed 7 cm upstream from the vane leading edge plane. The grid generated turbulence condition is developed by placing a rectangular duct containing a grid in between the exit of the nozzle and the entrance to the cascade. The square bar square mesh grid consists of a 1.27 cm aluminum bar spaced at 6.35 cm, producing a turbulence level of about 8.5% with a scale of about 3.5 cm at the measuring plane. The aerocombustor turbulence condition is generated by replacing the nozzle with a combustor simulator, which is described by Ames et al. [23]. Inlet boundary layer parameters for the low turbulence case and the aerocombustor case were previously reported by Ames et al. [24].

3.3 Cascade Test Section. The cascade test section shown schematically in Fig. 2 is configured with four vanes and three full passages. The aerodynamic or heat transfer test vane is located third from the bottom, to reduce the influence of the boundary layer growth along the bottom tailboard. The cascade test section has inlet bleeds designed along inlet streamlines, which are used together with an inlet row of static pressure taps to develop good inlet uniformity. The test section also has flexible tailboards extending from the trailing edge of the top and bottom vanes. The tailboards are used with the exit row of static pressure taps, located 1/4 axial chord downstream from the vane trailing edge plane, to develop good exit periodicity. The two-axis traversing system sits at the exit of the cascade and positions a 4.76 mm diameter five-hole cone probe across the passage downstream from the test vane. The traversing plane is parallel to the exit of the cascade or approximately perpendicular to the exit flow direction. The traversing plane is located at a position downstream from the test vane trailing edge, where the nominal flow direction intersects with the a line located 1/4 axial chord from the trailing edge exit plane. The approximate traversing location is shown in Fig. 2.

3.4 Letterbox Vane and Pressure Distributions. A cross-sectional view of the letterbox aerovane is shown in Fig. 3. The vane has a true chord of 47.8 cm and an axial chord of 25.0 cm. The leading edge diameter is 5.59 cm and the trailing edge diameter is 0.98 cm. The circumferential spacing of the vanes is 38.39 cm and the measured exit angle ranges from about 73 deg to 74 deg. The schematic shows the location of the surface and inner suction surface pressure taps, the coolant feed tube, the wooden pin conditioning section, the five-row converging pin fin array, and the letterbox partitions. Coolant discharge flow enters the vane through the coolant discharge tube, which has a contracting flow area from inlet to tip, and leaves through ten discharge holes.

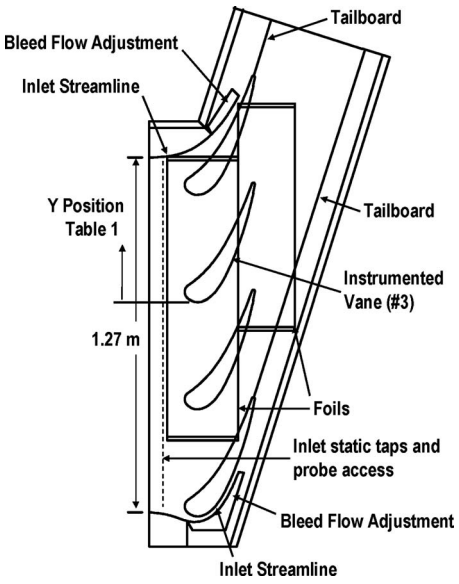

Fig. 2 Schematic of 11 times scale cascade test section

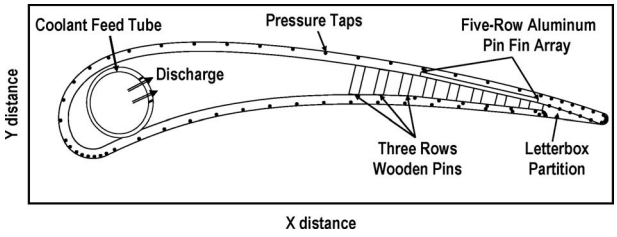

Fig. 3 Schematic of cross section for letterbox pressure vane

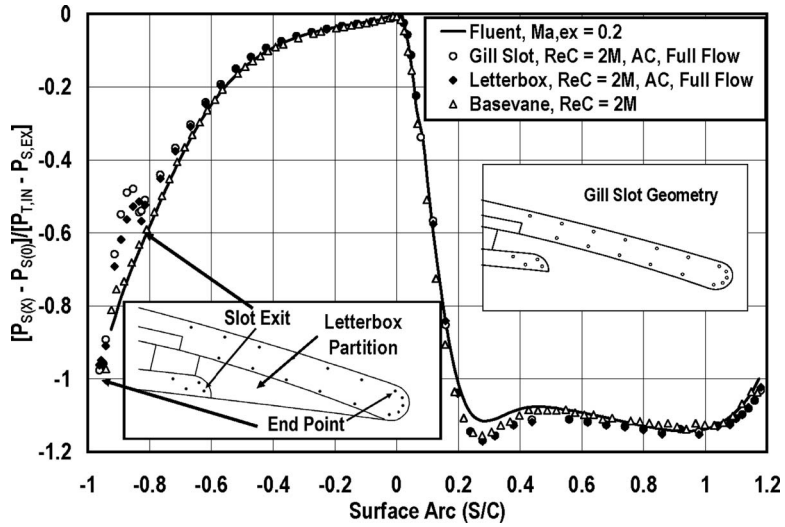

Fig. 4 Surface pressure distribution comparison for base, gill slot, and letterbox vanes, Re_C=2,000,000

The flow then is directed toward the three-row wooden pin conditioning section prior to the five-row converging pin fin array. The staggered pin fin array has an entrance height of 1.872 cm and an exit height of 0.653 cm. The pins are 0.84 cm in diameter and are spaced in the spanwise and streamwise direction at 2.5 pin diameters. The round leading edge of the partitions is located 1.5 diameters downstream from the trailing edge of the last pin row. The partitions are 0.635 cm thick and are spaced in the centerline between the last row of upstream pin fins. The radius of the pressure surface discharge slot lip is 0.56 cm and the exit slot is 0.56 cm in height. Pressure taps on the inner suction surface are placed midspan between the partitions.

The letterbox aerodynamic vane has 65 surface static pressure taps cast into the vane to sense the midspan surface pressure distribution presented in Fig. 4. In this figure, the local surface static pressure less the stagnation pressure normalized on the inlet total to average exit static pressure is plotted as a function of surface arc normalized by chord length. The figure presents the calculated surface pressure distribution compared with the experimental base vane, gill slot, and letterbox vane pressure distributions taken at a chord Reynolds number of 2,000,000 and at design flow. The profile for this incompressible vane was designed by Rolls-Royce (of North America) to have a fully loaded pressure distribution similar to fully loaded compressible flow vanes. The comparison between base vane and FLUENT [25] calculation shows good agreement, indicating that the midspan cascade aerodynamics provide a good representation of the 2D blade to blade flow solution. The gill slot and letterbox distributions agree quite well with the calculated and measured pressure distributions for the base vane except for the region near and downstream of the coolant discharge slot. In this region the gill slot and letterbox vane pressure distributions vary significantly from the base vane profile. The pressure distribution initially produces a significant pressure recovery directly downstream of the discharge exit and then rapidly accelerates toward the trailing edge. An insert showing the location of the pressure taps downstream of the slot is shown in Fig. 4, for the letterbox configuration. An insert is also shown for the gill slot or cut back trailing edge.

A comparison of the letterbox (open symbols, solid lines) and gill slot (solid symbols, dashed lines) pressure distribution downstream from the discharge slot is presented in Fig. 5. The normalized pressure in this figure is the same as in Fig. 4 but the surface

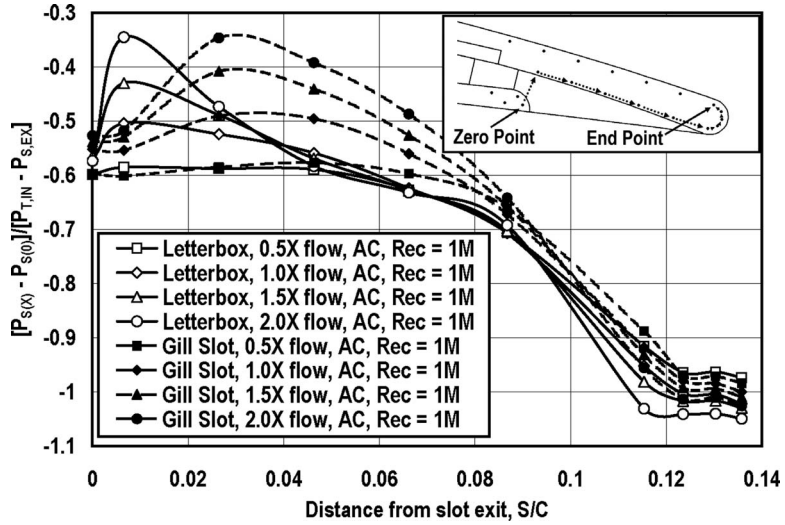

Fig. 5 Pressure surface discharge static pressure comparison for letterbox and gill slot vanes

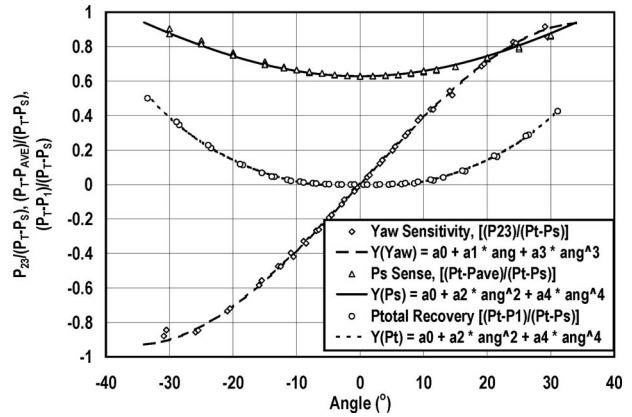

Fig. 6 Five-hole cone probe sensitivity for yaw angle, static pressure, and total pressure recovery, Re_C=2,000,000

distance starts from the last pressure tap on the pressure surface. The letterbox data generally show a significant rise in pressure between the last point on the pressure surface and the first point on the inner suction surface. Thereafter, the pressure distribution shows a strong favorable pressure gradient to the trailing edge. The last tap on the pressure surface and the first tap on the inner suction surface show consistent levels of pressure for the gill slot vane over the range of flow rates tested. However, as the discharge flow continues downstream the pressure shows a strong recovery before a strong favorable pressure gradient to the trailing edge. The pressure recovery downstream of the slot is similar on both vanes but the location is further downstream on the gill slot vane.

3.5 Exit Surveys. Exit surveys of total pressure loss, flow angle, and velocity were acquired downstream from the instrumented aerodynamic vane using a 60 deg included angle five-hole cone probe. The 4.76 mm diameter probe was calibrated for both pitch and yaw over a ± 25 deg angle in both directions for the three exit velocities. The calibration for the 2,000,000 chord Reynolds number surveys is presented in Fig. 6 and shows the angle or yaw sensitivity, the average to static pressure, and the total pressure recovery coefficients. Generally, except in rare cases, the cone of the probe stays within 10 deg of the flow direction. In this range the angle sensitivity coefficient is very linear and determining the flow angle from the cross-port pressure difference is both accurate and straight forward. Generally, the total pressure sensitivity is quite flat in this range and close to zero. While the average to static pressure coefficient is sensitive to the angle in this range, the resulting uncertainty has little influence on the total pressure losses, secondary velocities, and turning angle distributions reported in this paper.

The four pressure ports that are placed symmetrically on the cone downstream from the tip are sensed independently using miniature amplified peizoresistive pressure sensors. These downstream ports on the cone probe are all referenced to the center port. The difference in total pressure between the cascade inlet total pressure probe and the center port is sensed with a fifth miniature peizoresistive pressure sensor. Miniature pressure sensors with a 5000 Pa full scale range were used for the 2,000,000 chord exit Reynolds number traverses, and 1250 Pa full scale sensors were used for the 1,000,000 and 500,000 Reynolds number cases. The traversing position of the probe tip was set at the downstream position where a line from the vane trailing edge in the nominal flow direction intersected with a plane 1/4 axial chord downstream from the vane trailing edge plane. This location placed the probe 11.67 cm downstream from the vane trailing edge in the flow direction. The two-axis traversing system, which sat at the exit of the cascade, was used to traverse the probe from 4.76 mm above the endwall surface to midspan and across one passage centered around the vane trailing edge. Each traverse consisted of 27 positions in the spanwise direction and 25 positions in the circumferential direction. The pressures lines contained restrictions to dampen pressure fluctuations and each port at each position was read from between 25 and 75 times in order to provide statistically resolved mean values. Additionally, the pitch angle was corrected for the wall normal shear gradient and the loss in the endwall boundary layer was accounted for by using Spalding's law of the wall [26] profile.

3.6 Data Acquisition System. The PC based data acquisition system included a 100 channel HP 3497A, a custom made pressure scanner using two Rosemount pressure transmitters, two arrays of Allsensor miniature amplified piezoresistive pressure sensors, type K fine wire thermocouples, and a two-axis traversing system positioned by two Unislide lead screw drive tables. The HP 3497A was used to acquire all the pressure and thermocouple voltages using its integral voltmeter with 1 μV sensitivity set to integrate over 1 power line cycle. The custom made scanner used to acquire cascade test section pressures included two Rosemount pressure sensors connected in parallel and having full scale ranges of 250 Pa and 5000 Pa. The most sensitive sensor within range was used to determine each pressure. A 25 s settling time was used for all measurements, and voltages were typically averaged over 20 readings. The 5000 Pa and 1250 Pa Allsensor piezoresistive pressure sensor arrays used with the cone probe were powered using a 5 volts DC Acopian power supply and zeroed using a 1000 Ω potentiometer. The fine wire thermocouples used to determine inlet total and coolant flow air temperatures were referenced to a passive constant temperature reference junction using an ice bath. The fine thread lead screw drive tables were actuated using stepper motors, which were controlled with an Anaheim automation stepper motor controller and power supply.

3.7 Experimental Uncertainties. Estimates for uncertainty in the reported values of Ω, the total pressure loss coefficient, β, the turning angle, and $[P_{S(X)}-P_{S(0)}]/[P_{T,\mathrm{IN}}-P_{S,\mathrm{EX}}]$, the normalized vane surface pressure, were calculated using the root sum square method described by Moffat [27]. Based on a perturbation of the data reduction program, uncertainty in the normalized vane static pressure, $[P_{S(X)}-P_{S(0)}]/[P_{T,\mathrm{IN}}-P_{S,\mathrm{EX}}]$, was 0.02. Uncertainty in the local loss coefficient Ω was as high as 0.01 for the aerocombustor low Reynolds number case and 0.008 for the low turbulence case. This value was largely due to the relative bias error in the pressure measurement at the low Reynolds number, which was 0.0075 of the dynamic pressure. Uncertainty in the relative bias error was estimated to be 0.0015 for the higher Reynolds numbers. Uncertainty in the local angle included bias errors, unsteadiness error, and probe setup error. The maximum bias error was 0.26 deg for the low Reynolds number. The maximum unsteadiness error was 0.25 deg and roughly equal for all Reynolds numbers for the high turbulence condition. The maximum error in the setup angle was estimated to be only 0.20 deg as the angle of the probe could be referenced to the cascade using high resolution digital images. Also, it should be noted that all exit surveys had the same setup. The uncertainty in reported turbulence level is estimated to be 3% of the reported value. The experimental error in turbulent scale is estimated to be 11%. All uncertainty estimates are quoted at 95% confidence intervals.

4 Experimental Results

The objective of the exit survey measurements was to provide a basis for the comparison of losses between different trailing edge cooling configurations. Previously, exit survey loss measurements were conducted on the base [22] and gill slot [23] vanes over a range of Reynolds numbers (500,000, 1,000,000 and 2,000,000), turbulence conditions (low (0.7%), grid (8.5%), and aerocombustor (13.5%)), and in the case of the gill slot vane over a range of design flow rates. In order to provide the most useful compari-

Table 2 Summary of letterbox vane exit losses and turning angle at full design flow and off design flows

1/4 C_{AX}	Aerocombustor			Low turbulence			Grid turbulence		
File	exsvlbac53	exsvlbac13	exsvlbac23	exsvlblt53	exsvlblt13	exsvlblt23	exsvlbgt53	exsvlbgt13	exsvlbgt23
$Re_{C,EX}$	510,231	1,014,509	2,002,773	500,344	1,003,353	2,006,766	502,455	1,000,178	1,998,762
$T_{T,IN}$ (K)	291.6	293.0	298.6	294.2	294.9	300.9	288.0	298.7	297.6
$P_{T,IN}$ (Pa)	98,532	100,156	100,216	100,533	99,358	100,116	99,852	100,320	100,239
V_{EX} (m/s)	16.42	32.61	68.68	16.02	32.88	69.87	15.60	33.22	68.06
Ma_{EX}	0.0479	0.0950	0.1975	0.0466	0.0954	0.2002	0.0458	0.0958	0.1961
Ω (full)	0.0836	0.0650	0.0602	0.0563	0.0456	0.0466	0.0638	0.0555	0.0516
Ω (midline)	0.0717	0.0561	0.0515	0.0599	0.0360	0.0363	0.0501	0.0446	0.0407
β (full)	73.18	73.70	73.76	73.28	73.53	73.62	73.25	73.66	73.57
β (midline)	72.91	73.39	73.67	73.22	73.96	74.07	73.60	73.87	74.16
M_{DOT} (kg/s)	0.0135	0.0272	0.0542	0.0133	0.0270	0.0555	0.0142	0.0261	0.0548
T_{ORF} (K)	288.5	293.7	300.0	292.8	294.6	298.1	290.4	296.1	296.3
ΔP_{ORF} (Pa)	72.9	298.4	1201.0	70.6	296.8	1265.6	80.5	277.0	1211.0
P, atm (Pa)	99,311	99,751	98,498	100,428	98,938	97,550	100,225	99,886	98,532

1/4 C_{AX}	Aerocombustor			Low turbulence		
File	exsvlbac513	exsblbac313	exsvlbac213	exsvlblt513	exsvlblt313	exsvlblt213
$Re_{C,EX}$	1,002,227	1,017,136	997,004	1,004,601	1,028,110	1,005,902
$T_{T,IN}$ (K)	297.2	296.9	296.8	295.3	294.5	299.3
$P_{T,IN}$ (Pa)	99.499	99.495	99.278	100,137	100,892	98,662
V_{EX} (m/s)	33.26	33.71	33.08	32.75	33.12	34.12
Ma_{EX}	0.0962	0.0975	0.0957	0.0950	0.0962	0.0983
Ω (full)	0.0651	0.0530	0.0415	0.0463	0.0390	0.0212
Ω (midline)	0.0558	0.0439	0.0311	0.0372	0.0306	0.0083
β (full)	73.61	73.68	73.71	73.52	73.54	73.70
β (midline)	73.35	73.48	73.50	73.97	74.05	73.94
M_{DOT} (kg/s)	0.0132	0.0415	0.0539	0.0137	0.0399	0.0543
T_{ORF} (K)	296.8	291.3	294.3	293.1	296.2	297.3
ΔP_{ORF} (Pa)	71.1	690.4	1164.1	75.9	640.7	1199.2
P, atm (Pa)	99,074	99,074	98,871	99,717	100,462	98,227

sons, the letterbox vane was run at the same coolant flow rates as the gill slot vane. The design flow rate for the gill slot vane was determined as the flow produced through the converging pin fin array and discharge from 2/3 of the pressure drop normally available to the first vane from the compressor to the exit of the gill slot [23]. At an exit chord Reynolds number of 1,000,000 design flow is nominally 0.027 kg/s or about 2.54% of passage flow. Since the minimum exit slot flow area is reduced by 30% due to the letterbox partitions, the nominal pressure drop across the converging pin fin array and letterbox discharge has also increased. Based on pressure drop measurements [1], this increase averages about 30%. A tabulation of the exit survey conditions and loss parameters is presented in Table 2 for design flow conditions and Table 2 for off design flow conditions.

4.1 Exit Survey Loss Contours and Secondary Flows. Exit survey loss contours and secondary flows are presented in this section for the letterbox vane. However, in order to present a clearer picture of the impact of the letterbox geometry, loss contours for the letterbox vane are compared with loss contours for the base and gill slot vanes. Note that comparisons will be made on an incremental basis, which means that an increase in total pressure losses from 5.1% to 5.5% would in an incremental increase of 0.4%. Figure 7(*a*) presents loss contours for the base vane at an exit chord Reynolds number of 1,000,000 at the low turbulence condition. The surveys were taken across one full passage and half the span. The wake of the base vane is quite thin and appears largely two dimensional at this condition. The thin wake results from the presence of a laminar boundary layer developing on the suction surface. A endwall loss core is also present and the core has been convected about 4.6 cm or about 18% span above the endwall. The position of the endwall loss core is likely a result of the inlet boundary layer thickness [28], which is relatively thin [24]. The characteristic over turning near the endwall is visible but relatively weak, and evidence of a corner vortex is also present in the wake near the endwall. Secondary loss contours are presented in Fig. 7(*b*) for the gill slot vane also at an exit Reynolds number of 1,000,000 and at low turbulence. However, in Fig. 7(*b*) the gill slot vane is discharging coolant at the design flow rate. Qualitatively, Fig. 7(*b*) is quite similar to Fig. 7(*a*) for the base vane except for the much broader wake resulting from the gill slot with coolant discharge. The wake is consistently much broader and somewhat deeper across the entire span. The incremental loss increase from the base vane to the gill slot vane at design flow is 1.16%. The letterbox vane secondary loss contours shown in Fig. 7(*c*) are very similar to the gill slot vane at this low turbulence, design flow, and 1,000,000 Reynolds number condition. The width of the wake, the secondary flows, and the character of the losses are very similar. The incremental loss between the base vane and letterbox vane at design flow is about 0.9%. This slight reduction in loss from the gill slot vane is likely due to higher injection velocity at the design flow for the letterbox vane. However, the discharge flow around the letterbox partitions is likely an additional source of separation losses. Another aspect of the flow is the waviness of the side of the wake which is likely due to the interaction of the discharge flow, segmented with letterbox partitions, and the freestream.

Secondary loss contours for the gill and letterbox vanes are shown in Figs. 7(*d*) and 7(*e*) for the grid turbulence condition at the design flow rate and a chord Reynolds number of 1,000,000. The gill slot wake for the grid turbulence is much broader than the wake for the low turbulence condition. This broader wake is primarily due to the state of the suction surface boundary layer, which transitions to turbulent flow early on the suction surface. The characteristic over turning along the endwall has increased

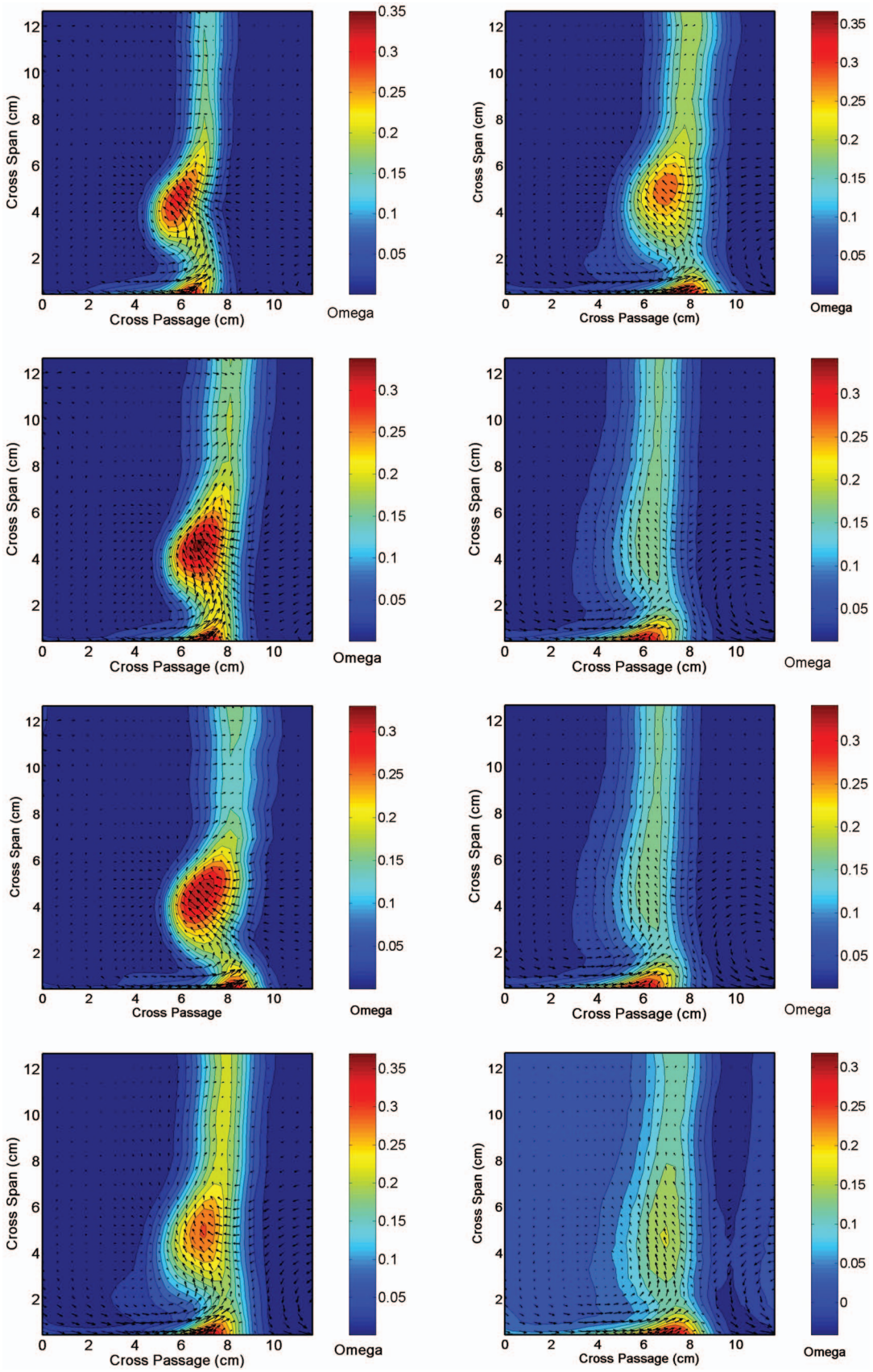

Fig. 7 Exit survey loss contours and secondary flows, Re_C=1,000,000: (*a*) base vane, low turbulence; (*b*) gill slot vane, full flow, low turbulence; (*c*) letterbox vane, full flow, low turbulence; (*d*) gill slot vane, full flow, grid turbulence; (*e*) letterbox vane, full flow, grid turbulence; (*f*) base vane, aerocombustor turbulence; (*g*) letterbox vane, full flow, aerocombustor turbulence; and (*h*) letterbox vane, 200% design flow, aerocombustor turbulence

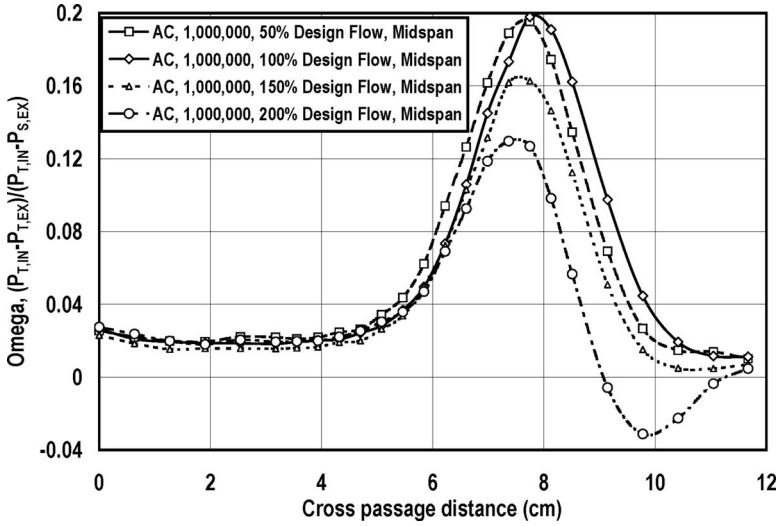

Fig. 8 Midspan total pressure loss coefficient Ω as a function of cross-passage distance for letterbox vane for varying design flow, AC, and Re_C =1,000,000

with the grid turbulence and the center of the endwall loss core is higher at 5 cm than the low turbulence condition. The passage averaged loss has increased by about 1% from the low turbulence condition to the grid turbulence condition due to the suction surface boundary layer. Additionally, the incremental loss for gill slot vane above the base vane for the grid condition is about 1.3%. Figure 7(*e*) presents the total pressure loss contour and secondary velocity vectors for the letterbox vane. This figure looks very similar to the plot for the gill slot vane. The edge of the contour plot may exhibit a little more waviness but the influence of the grid turbulence has largely masked the discrete nature of the letterbox discharge. The passage averaged loss was experimentally determined to be about 0.3% less, incrementally, than the loss for the gill slot vane for the same flow, turbulence, and Reynolds number condition.

Figures 7(*f*)–7(*h*) show total pressure loss contours for the aerocombustor condition. Figure 7(*f*) presents total pressure loss contours and secondary velocities for the base vane at a Reynolds number of 1,000,000. The aerocombustor loss contours show a substantially different character than either the low or grid generated turbulence condition. The wake is much broader and there is no indication of a discrete endwall loss core. The high intensity large-scale turbulence has moved the flow structures around and essentially blurred the presence of a loss core. The incremental losses for the base vane for the aerocombustor condition are 1.9% higher than the low turbulence condition due to a turbulent suction surface boundary layer, higher inlet losses, and turbulence mixing. The inlet velocity profile parameters have been documented [24] and the inlet momentum deficit is substantially larger for the aerocombustor as compared with the low turbulence case. The high turbulence mixing across velocity gradients around the vane is also responsible for a portion of the background loss seen in the region between wakes. The total pressure loss contours and secondary velocities for the letterbox vane at design flow, 1,000,000 Reynolds number, and aerocombustor turbulence are shown in Fig. 7(*g*). The character of the wake and secondary velocities is very similar to the base vane case. However, the wake is clearly much broader and somewhat deeper than the base vane with an incremental increase in about 0.9% in losses. Similar to the base vane the over turning along the endwall is strong due to the significant inlet boundary layer momentum loss.

At the design flow condition, the local discharge velocity to freestream velocity ratio is 0.9. However, at a flow rate of two times the design flow rate, the discharge to freestream velocity ratio is closer to 1.8. Figure 7(*h*) presents the letterbox vane at similar freestream conditions as Figs. 7(*f*) and 7(*g*) but at a flow rate two times the design flow. In this figure the character of the loss is much different than other figures due to the presence of a region with a total pressure noticeably higher than the low loss region between wakes. This figure indicates that the injection of the high momentum fluid tends to fill in the wake and results in a total pressure loss, which is 2.35% lower than the design flow passage averaged losses.

The midspan total pressure loss profile is presented as a function of fraction of design flow for the letterbox vane at the aerocombustor turbulence level and a 1,000,000 Reynolds number in Fig. 8. The wakes for the half and full design flows are very similar in peak deficits and wake widths with cross-passage averaged losses of 5.58% and 5.61%, respectively. The wakes are slightly shifted possibly due to the location of coolant injection. The 1.5 times design flow profile has a much lower peak deficit and a thinner wake with a cross-passage averaged loss of 4.39%. The higher momentum flow has clearly filled in a portion of the profile momentum deficit. The profile for the two times design flow not only shows a lower peak deficit and thinner wake but the profile also displays a region of negative total pressure loss parameter Ω due to the very high momentum discharge. The two times design flow case has a midspan cross-passage averaged loss of 3.11%. Typical first stage vane feed pressures are unlikely to be able to produce discharge velocities greater than the design flow condition. However, higher flow rates are quite possible for downstream vanes and blades.

4.2 Cross Passage Averaged Total Pressure Loss and Turning Angle. The total pressure loss coefficient Ω and the turning angle β were mass averaged in the cross-passage direction to provide a means to compare results from different conditions. Figure 9 presents the cross-passage averaged total pressure loss coefficient as a function of cross span distance for the letterbox vane comparing different turbulence conditions. The distributions were all taken at a chord Reynolds number of 1,000,000 at full design flow. The base vane distribution for the aerocombustor turbulence is shown for comparison. The nominal initial location off the wall is 4.76 mm or equivalent to the diameter of the cone probe, and the losses at this location are high. Near midspan, the profile losses are largely two dimensional and increase with increasing turbulence level. Significant loss peaks for the low and grid turbulence cases at 4.5–5 cm from the endwall correspond to the

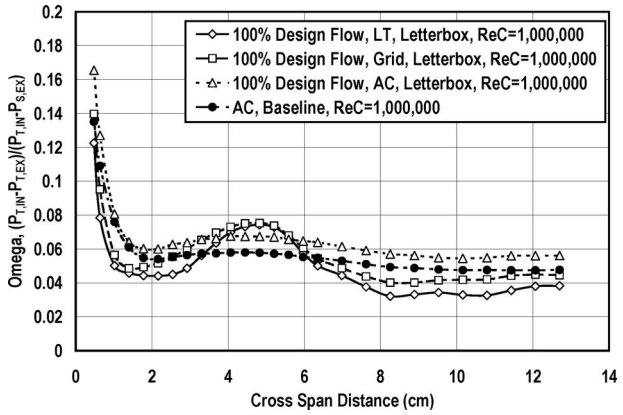

Fig. 9 Cross passage averaged total pressure loss coefficient Ω as a function of cross span distance for letterbox vane, varying turbulence intensity, design flow, and Re_C=1,000,000

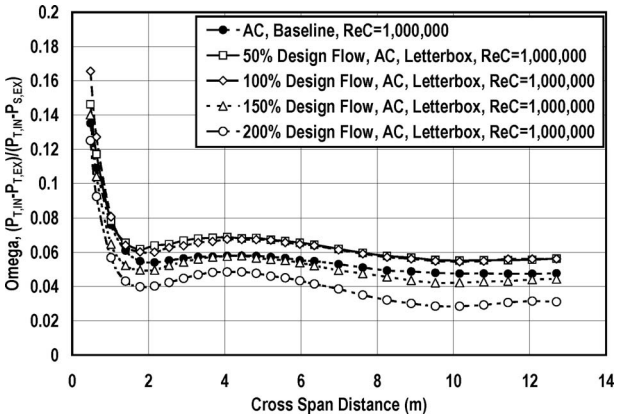

Fig. 11 Cross passage averaged total pressure loss coefficient Ω as a function of cross span distance for letterbox vane, varying design flow, AC, and Re_C=1,000,000

cross span location of the endwall loss core presented in the contour plots. The aerocombustor case does not have the same increase in this region due to the action of the large-scale turbulence redistributing the losses. However, a mild increase above the midspan level is present, which is spread throughout much of the lower span. The letterbox configuration for the aerocombustor turbulence shows an incremental increase in losses above the base vane case, which is almost uniform across the span of the vane. Figure 10 presents the spanwise distribution of cross-passage averaged total pressure loss distribution comparing the influence of Reynolds number. The distributions clearly show increasing losses with decreasing Reynolds number for the aerocombustor condition. Losses for the 2,000,000 Reynolds number case are only slightly higher than for the base vane at a Reynolds number of 1,000,000. The character of the distributions is very similar. The influence of percent design flow rate on the spanwise distribution of total pressure loss is presented in Fig. 11 for the letterbox vane. The base vane distribution for the aerocombustor turbulence is shown for comparison. The level of losses is very similar for the half and full design flow distributions with a tradeoff between injection at a lower flow rate but at a higher momentum deficit versus a higher flow rate at a lower momentum deficit. The one and a half design flow case injects fluid with a higher momentum than the local freestream producing a loss lower than the base vane case. The two times design flow case consistently has the lowest loss across the span.

Secondary flows have a noticeable influence on the turning angle. Figure 12 presents the cross-passage averaged turning angle β as a function of cross span distance for the three turbulence conditions and the base vane at the aerocombustor condition. The three letterbox distributions were all acquired at full design flow, and all distributions were acquired at an exit chord Reynolds number of 1,000,000. The aerocombustor turbulence condition for both the base and letterbox vane has the highest near wall turning angle. As mentioned previously, this high level of overturning near the endwall is likely a result of the significant momentum loss in the cascade inlet boundary layer for this condition. The low turbulence condition has a much thinner inlet boundary layer and significantly reduced near endwall turning angle. Near 20% span (5 cm) the turning angle decreases due to the action of the passage vortex, which convects the endwall loss core up off the endwall and away from the suction surface. Near midspan the turning angle appears to be close to two dimensional. Also, in comparison with the base vane case the letterbox vane with design flow has a measurably higher turning angle. The influence of Reynolds number for the cross-passage averaged turning angle is presented in Fig. 13 for the aerocombustor condition. Generally, the passage averaged turning angle increases with increasing Reynolds number. This behavior is similar for all three turbulence conditions. Additionally, this increasing turning angle with increasing Reynolds number is also found, but to a lesser extent for the gill slot vane.

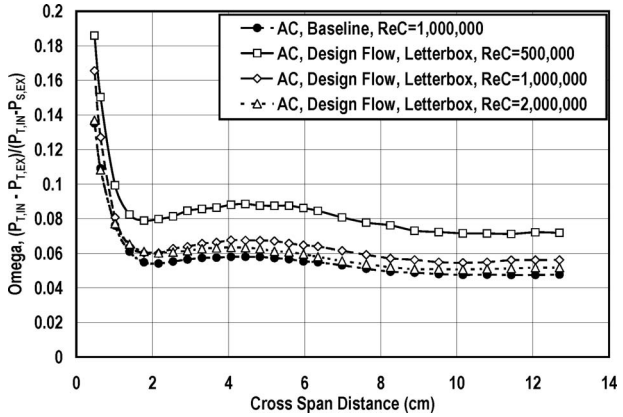

Fig. 10 Cross passage averaged total pressure loss coefficient Ω as a function of cross span distance, letterbox vane, design flow, AC, and Re_C=500,000, 1,000,000, and 2,000,000

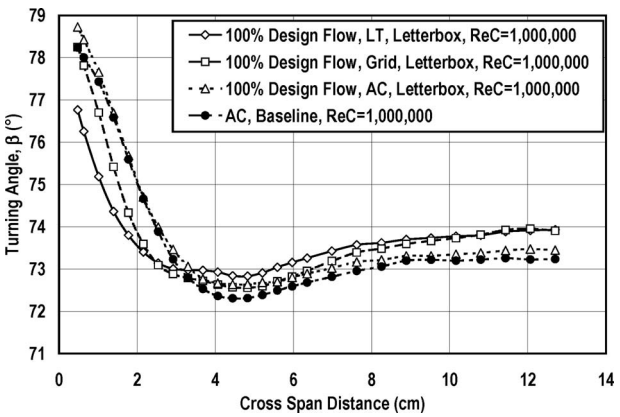

Fig. 12 Cross passage averaged turning angle β as a function of cross span distance for letterbox vane, comparing turbulence levels, design flow, and Re_C=1,000,000

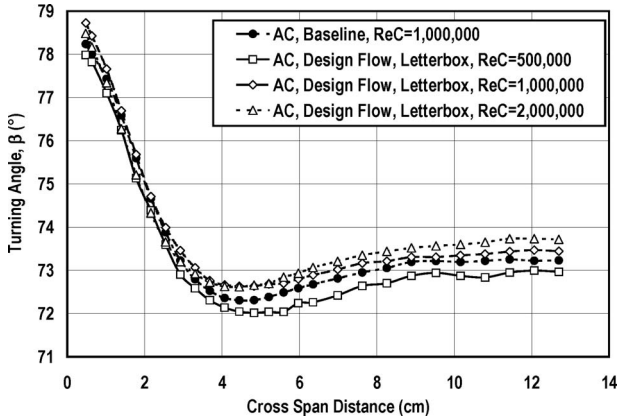

Fig. 13 Cross passage averaged turning angle β as a function of cross span distance for letterbox vane, design flow, AC, and Re_C=500,000, 1,000,000, and 2,000,000

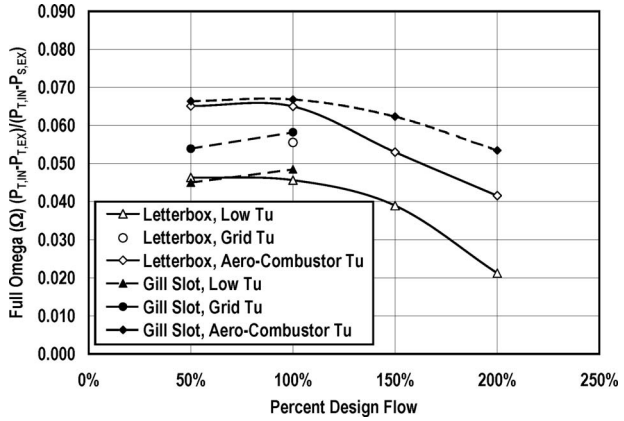

Fig. 15 Full passage averaged total pressure loss coefficient Ω as a function of percent design flow and turbulence condition, letterbox and gill slot vanes, and Re_C=1,000,000

4.3 Passage Averaged Total Pressure Loss Coefficients. Mass averaging the total pressure loss coefficient across the entire passage provides a means for comparison between different conditions and geometries. Figure 14 presents the passage averaged total pressure loss coefficient as a function of Reynolds number comparing losses for the letterbox and gill slot vanes for the low, grid, and aerocombustor turbulence conditions. The figure shows some general trends including decreasing losses with increasing Reynolds number, increasing losses with increasing turbulence level, and a slight reduction in losses with the letterbox geometry. The letterbox geometry has a smaller exit area and for the same flow, the coolant is discharged with a higher momentum. The letterbox geometry also has partitions segmenting the slot and providing an additional region where flow separates and where fluid from two streams can mix. This increased momentum is likely responsible for the slightly reduced loss for the letterbox geometry at the design flow. Across the three Reynolds numbers and three turbulence conditions, the letterbox vane's incremental passage averaged total pressure loss coefficient is about 0.2% less than the gill slot vane value.

The discharge flow rate was also found to have a significant influence on the passage averaged total pressure loss for a given condition. The passage averaged total pressure loss as a function of relative discharge flow rate is presented in Fig. 15 for the gill slot and letterbox vane for the three turbulence conditions. The data are presented for a chord Reynolds number of 1,000,000. The response as a function of flow rate is relatively flat at the 50% and 100% design flows likely due to a tradeoff between reduced momentum deficit and increased discharge flow with higher relative cooling discharge rates. A substantial reduction in total pressure losses occurs with increasing coolant discharge above the design flow as discharge momentum exceeds that of the local freestream. At the aerocombustor condition, where the only comparison across the full range of flow can be made, a noticeably larger reduction in losses occurs for the letterbox vane. This difference in losses is likely a function of the increased letterbox discharge velocity for a given flow.

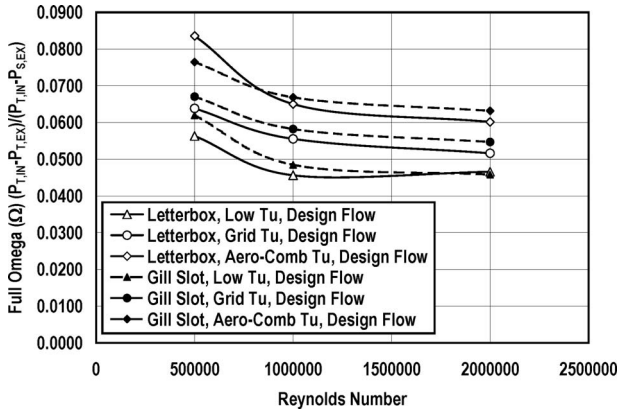

Fig. 14 Full passage averaged total pressure loss coefficient Ω as a function of exit chord Reynolds number and turbulence condition, letterbox and gill slot vanes, and design flow

5 Summary and Conclusions

Full exit surveys of total pressure loss and turning angle were acquired for a letterbox geometry across a range of exit chord Reynolds numbers (500,000, 1,000,000, and 2,000,000), over varying coolant discharge flow rates (50%, 100%, 150%, and 200% design flows), and with low (0.7%), grid (8.5%), and aerocombustor (13.5%) turbulence conditions. Additionally surface pressure distributions have also been documented. These measurements have been compared with base vane and gill slot vane measurements. In a related paper [1], heat transfer and adiabatic effectiveness measurements have been documented for the letterbox vane on the partitions and in the discharge area.

Letterbox surface pressure distributions varied significantly from the base vane only in the discharge area. Similar to the gill slot vane pressure distributions in this region were a strong function of the coolant discharge flowrate.

The letterbox vane produced an incremental increase in loss over the base vane for all conditions and generally produced incremental losses of about 0.2% less than the gill slot vane at the same conditions. Generally, passage averaged losses decreased with increasing Reynolds number. Also, at flow rates greater than the design flow, losses decreased with increasing discharge flow.

The letterbox vane showed increasing turning angle at increasing Reynolds numbers. Also, at the design flow discharge the letterbox vane had a higher turning angle than the base vane at similar conditions.

These results provide designers with incremental losses for varying turbulence levels, Reynolds numbers, and coolant discharge. This study also allows designers to directly compare aerodynamic losses between different trailing edge cooling schemes.

Acknowledgment

The authors gratefully acknowledge the support from the University Turbine System Research (UTSR) consortium, which is administrated by the South Carolina Institute for Energy Studies and largely funded through DOE's National Energy Technology

Laboratory. The authors would also like to acknowledge the help of Rolls-Royce of North America for providing the vane geometry used in this study. Additionally, the facility used in this project was funded through a seed grant from the North Dakota EPSCoR program. In addition, the authors are indebted to the University of North Dakota for providing additional support and laboratory space.

Nomenclature

- C = vane true chord length, m
- C_{AX} = axial chord length, m
- Lu = energy scale, $\text{Lu}=1.5|u'|^3/\varepsilon$
- Lx = longitudinal integral scale of u' fluctuation
- M_{DOT} = coolant mass flow rate, kg/s
- P = pressure, Pa
- Re_C = Reynolds number based on true chord and exit conditions
- S = vane surface arc length measured from stagnation point, m
- T = temperature, K
- Tu = turbulence level, $\text{Tu}=|u'|/U_\infty$
- U = freestream velocity, m/s
- $u', |u'|$ = streamwise component rms fluctuation velocity, m/s
- V_{EX} = cascade exit velocity, m/s
- X = surface location from the leading edge

Greek Letter Symbols

- β = turning angle, deg
- ε = turbulent dissipation rate, m^2/s^3
- Ω = total pressure loss coefficient, $[P_{T,\text{IN}}-P_{T,\text{EX}}]/[P_{T,\text{IN}}-P_{S,\text{EX}}]$, also omega

Subscripts

- CO = refers to conditions at the letterbox slot exit
- EX = refers to conditions at the nozzle exit plane
- IN = refers to conditions at the nozzle inlet plane
- ORF = refers to conditions at the orifice
- S = refers to static condition
- T = refers to total or stagnation condition
- ∞ = evaluated in the freestream

References

[1] Fiala, N. J., Johnson, J. D., and Ames, F. E., 2008, "Letterbox Trailing Edge Heat Transfer—Effects of Blowing Rate, Reynolds Number, and External Turbulence on Heat Transfer and Film Cooling Effectiveness," ASME Paper No. GT2008-50474.
[2] Denton, J. D., 1993, "Loss Mechanisms in Turbomachines," ASME J. Turbomach., **115**, pp. 621–656.
[3] 1972, *Turbine Design and Application*, Vols. 1–3, A. G. Glassman, ed., Washington, DC, NASA SP-290.
[4] Gregory-Smith, D. G., and Cleak, J. G. E., 1992, "Secondary Flow Measurements in a Turbine Cascade With High Inlet Turbulence," ASME J. Turbomach., **114**, pp. 173–183.
[5] Ames, F. E., and Plesniak, M. W., 1997, "The Influence of Large Scale, High Intensity Turbulence on Vane Aerodynamic Losses, Wake Growth, and Exit Turbulence Parameters," ASME J. Turbomach., **119**, pp. 182–192.
[6] Ames, F. E., 1994, "The Influence of High Intensity, Large Scale Turbulence on Turbine Vane Heat Transfer and Aerodynamics," NASA Report No. CR 4633.
[7] Sieverding, C. H., 1985, "Recent Progress in the Understanding of Basic Aspects of Secondary Flow in Turbine Blade Passages," ASME J. Eng. Gas Turbines Power, **107**, pp. 248–257.
[8] Klein, A., 1966, "Investigation of the Entry Boundary Layer on the Secondary Flows in the Blading of Axial Turbines, BHRA Report No. T 1004.
[9] Langston, L. S., Nice, M. L., and Hooper, R. M., 1977, "Three-Dimensional Flow Within a Turbine Cascade Passage," ASME J. Eng. Power, **99**, pp. 21–28.
[10] Marchal, P., and Sieverding, C. H., 1977, "Secondary Flows Within Turbomachinery Bladings," Secondary Flows in Turbomachines, AGARD Paper No. CP 214.
[11] Praisner, T. J., and Smith, C. R., 2005, "The Dynamics of the Horseshoe Vortex and Associated Endwall Heat Transfer, Part I—Temporal Behavior," ASME, Paper No. GT2005-69088.
[12] Burd, S. W., and Simon, T. W., 2000, "Flow Measurements in a Nozzle Guide Vane Passage With a Low Aspect Ratio and Endwall Contouring," ASME J. Turbomach., **122**, pp. 659–666.
[13] Zess, G. A., and Thole, K. A., 2001, "Computational Design and Experimental Evaluation of Using an Inlet Fillet on a Gas Turbine Vane," ASME Paper No. 2001-GT-404.
[14] Ingram, G., Gregory-Smith, D., Rose, M., Harvey, N., and Brennan, G., 2002, "The Effect of End-Wall Profiling on Secondary Flow and Low Development in a Turbine Cascade," ASME Paper No. GT2002-30339.
[15] Kapteijn, C., Amecke, J., and Michelassi, V.,1994, "Aerodynamic Performance of a Transonic Turbine Guide Vane With Trailing Edge Coolant Ejection: Part I—Experimental Approach," ASME Paper No. 94-GT-288.
[16] Osnaghi, C., Perdichizzi, A., Savini, M., Harasgama, P., and Lutum, E., 1997, "The Influence of Film Cooling on the Aerodynamic Performance of a Turbine Nozzle Guide Vane," ASME Paper No. 97-GT-522.
[17] Pappu, K. R., and Schobeiri, M. T., 1997, "Optimization of Trailing Edge Ejection Mixing Losses: A Theoretical and Experimental Study," ASME Paper No. 97-GT-523.
[18] Deckers, M., and Denton, J. D., 1997, "The Aerodynamics of Trailing-Edge-Cooled Transonic Turbine Blades: Part 1—Experimental Approach," ASME Paper No. 97-GT-518.
[19] Uzol, O., and Camci, C., 2001, "Aerodynamic Loss Characteristics of a Turbine Blade With Trailing Edge Coolant Ejection: Part 2—External Aerodynamics, Total Pressure Losses, and Predictions," ASME J. Turbomach., **123**, pp. 249–257.
[20] Telisinghe, J. C., Ireland, P. T., Jones, T. V., Barrett, D., and Son, C., 2006, "Comparative Study Between a Cut-Back and Conventional Trailing Edge Film Cooling System," ASME Paper No. GT2006-91207.
[21] Brundage, A. L., Zucrow, M. J., Plesniak, M. W., Lawless, P. B., and Ramadhyani, S., 2007, "Experimental Investigation of Airfoil Trailing Edge Heat Transfer and Aerodynamic Losses," Exp. Therm. Fluid Sci., **31**(3), pp. 249–260.
[22] Ames, F. E., Johnson, J. D., and Fiala, N. J., 2006, "The Influence of Aero-Derivative Combustor Turbulence and Reynolds Number on Vane Aerodynamic Losses, Secondary Flows, and Wake Growth," ASME Paper No. GT-2006-90168.
[23] Ames, F. E., Johnson, J. D., and Fiala, N. J., 2007, "Gill Slot Trailing Edge Heat Transfer—Effects of Blowing Rate, Reynolds Number, and External Turbulence on Heat Transfer and Film Cooling Effectiveness," ASME Paper No. GT2007-27397.
[24] Ames, F. E., Barbot, P. A., and Wang, C., 2003, "Effects of Aeroderivative Combustor Turbulence on Endwall Heat Transfer Distributions Acquired in a Linear Vane Cascade," ASME J. Turbomach., **125**, pp. 210–220.
[25] 2001, FLUENT 6.0 User's Guide, Fluent, Inc., Lebanon, NH.
[26] White, F. M., 1991, *Viscous Fluid Flow*, 2nd ed., McGraw-Hill, New York.
[27] Moffat, R. J., 1988, "Describing the Uncertainties in Experimental Results," Exp. Therm. Fluid Sci., **1**, pp. 3–17.
[28] Ames, F. E., Hylton, L. D., and York, R. E., 1986, Unpublished work on the impact of the inlet endwall boundary layer on secondary losses and velocity vectors in a compressible turbine cascade, Allison Gas Turbine Division of General Motors.